ACS Energy LETTERS

Cite This: ACS Energy Lett. 2017, 2, 2299-2306

http://pubs.acs.org/journal/aelccp

LETTER

Crystallographic Data Support the Carousel Mechanism of Water Supply to the Oxygen-Evolving Complex of Photosystem II

Jimin Wang,[‡] Mikhail Askerka,[†] Gary W. Brudvig,[†] and Victor S. Batista*[,†]

[‡]Department of Molecular Biophysics and Biochemistry, Yale University, New Haven, Connecticut 06520-8114, United States

[†]Department of Chemistry, Yale University, New Haven, Connecticut 06520-8107, United States

Supporting Information

ABSTRACT: Photosystem II (PSII) oxidizes water to produce oxygen through a four-step photocatalytic cycle. Understanding PSII structure−function relations is important for the development of biomimetic photocatalytic systems. The quantum mechanics/molecular mechanics (QM/MM) analysis of substrate water binding to the oxygen-evolving complex (OEC) has suggested a rearrangement of water ligands in a carousel mechanism around a key Mn center. Here, we find that the most recently reported X-ray free-electron laser (XFEL) crystallographic data obtained for the dark-stable S_1 state and the doubly flashed S_3 state at 2.25 Å resolution support the carousel mechanism. The features in the XFEL data and QM/MM model-simulated difference Fourier maps suggest that water displacement may occur from the so-called "narrow" channel, resulting in binding of a new water molecule to the OEC, and thus provide new insights into the nature of rearrangements of water ligands along the catalytic cycle before O═O bond formation.

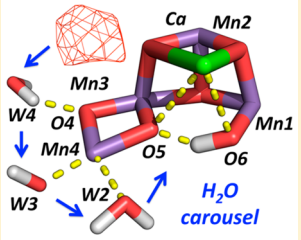

Photosystem II (PSII) is a large multisubunit membrane protein complex, responsible for direct solar water oxidation in higher plants, algae, and cyanobacteria.[1−3] Water is oxidized at the oxygen-evolving complex (OEC) embedded in the D1 protein subunit, an oxomanganese cluster that operates by cycling through five redox states, the so-called "storage states" (or "S states") of oxidizing equivalents (S_0−S_4). During each turn of the catalytic cycle, the OEC binds two water molecules and gets oxidized four times, generating the S_4 state that catalyzes O−O bond formation for O_2 evolution. While S_0 is the most reduced state, S_1 is the stable dark-adapted form of the OEC from which the S_4 state is formed after three flashes of light, leading to O_2 evolution and regeneration of the OEC in the S_0 state.[4,5] Structural models based on quantum mechanics/molecular mechanics (QM/MM) have been proposed for the S_0−S_3 states, consistent with known biochemical, spectroscopic, and crystallography data (Figure 1, Supporting Information (SI)).[6−11]

The QM/MM models suggest water binding to the cluster in the $S_2 \rightarrow S_3$ transition by a carousel rearrangement of water ligands around Mn4 (Scheme 1).[12] Here, we find that experimental data support such a carousel mechanism from the most recently reported X-ray free-electron laser (XFEL) crystallographic experiments,[13] which are the focus of this study. As discussed previously,[12] the narrow water channel has been considered by several groups as a water delivery pathway based on a variety of studies.[14−20] Alternative mechanisms,[21,22] including the pivot mechanism,[23] have also been proposed and claimed to be consistent with the XFEL data for the S_3 state.[13] Reference 21 disfavored the carousel mechanism on the basis of high-energy barriers for TS6 and TS7, although the pathway of the carousel corresponds to their TS4, which has a very low barrier. At the same time, we question whether the S_3 XFEL data have actually resolved the ambiguity of the water oxidation mechanism.

A number of X-ray crystallography models of PSII have been reported in recent years, including PSII models with the OEC in the S_1 state based on conventional synchrotron data.[24,25] However, data collection from conventional synchrotron sources has been shown to induce radiation damage of the OEC and formation of noncatalytically relevant reduced states.[24,26,27] X-ray radiation is thought to reduce the OEC and induce oxygen additions to protein side chains through mechanisms of hydroxyl free radicals.[27−30] Thus, significant efforts are currently focused on XFEL crystallography.[13,31,32]

High-resolution XFEL diffraction data have been collected using continuous translation of unexposed parts of large single crystals of PSII,[31] in an effort to achieve "diffraction-before-destruction". However, several technical aspects remain challenging.[33,34] The most effective approach for suppressing radiation damage has been the "one-shot-per-crystal" method, as in recent XFEL studies of the S_1 state corresponding to the model reported for 5WS5 (of PDB accession number)[13] and earlier studies of the S_1 and S_3 states.[35−39] In one XFEL study,[35] an insufficient degree of isomorphism between the S_1 and S_3

Received: August 15, 2017
Accepted: September 7, 2017
Published: September 7, 2017

DOI: 10.1021/acsenergylett.7b00750
ACS Energy Lett. 2017, 2, 2299−2306

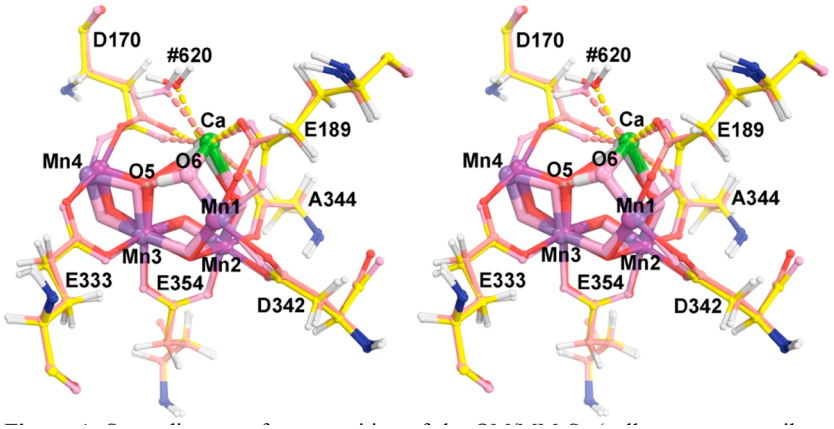

Figure 1. Stereodiagram of superposition of the QM/MM S_1 (yellow, magenta, silver, red, and blue) and S_3 (salmon, green, dark magenta, pink, and blue) models, including six bidentate carboxylate ligands to highlight the moving parts to be expected in difference density features.

Scheme 1. Carousel Mechanism for Supply of One of the Two Water Substrates to the OEC[a]

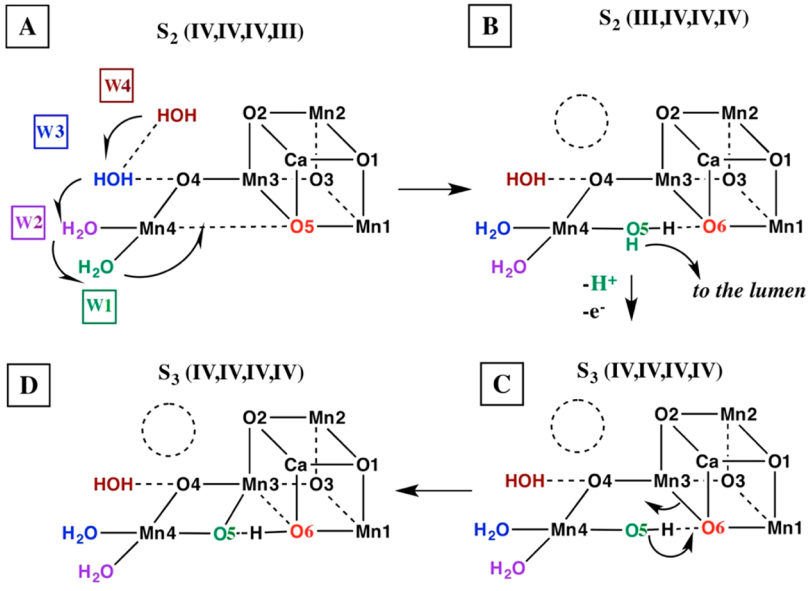

[a]Adapted from ref 12. (A) is the starting S_2 state, (D) is the final S_3 state, and (B) and (C) are proposed intermediate steps for the S_2 to S_3 state transition. W1, W2, and W3 correspond to W2, W1, and Wx in ref 12, respectively, while O5 has been relabeled as O6 following ref 13, after W1 moves into the O5 position to become O5.

states required computational realignment of the resulting electron density maps before difference electron density maps could be calculated and studied.[9] In other XFEL studies,[36−39] computational errors introduced by data reduction based on the software cctbx.xfel were so large that structural changes due to S_3 state formation were buried below the noise level.[40] Nonetheless, structural information associated with the S_1 to S_2 transition from noisy XFEL data could still be revealed for rearrangements that involved displacement of an Mn center, found to be consistent with the simulated Fourier difference maps predicted by QM/MM models.[8,36]

The recent XFEL study by Shen and co-workers reported high-quality data.[13] The data sets exhibit the highest possible isomorphism between the S_1 and S_3 states, with the overall amplitude and intensity isomorphous difference reported of only 6.8 and 5.6% at 2.35 Å resolution, respectively (see below for further discussion), ideally suitable for the observed isomorphous difference Fourier studies, that is, for calculation of the very sensitive F_{obs}(5WS6/S_3) − F_{obs}(5WS5/S_1) map or the F_{obs} − F_{obs} map (Figure 2A,B and SI).[41−43]

In particular, the dark-adapted S_1 structure[13] (PDB access code 5WS5) is found to be most consistent with EXAFS data (SI, Figure S1) and the previously proposed EXAFS-based[44] S_1 QM/MM model.[45] In contrast, the S_3 structure (PDB access code 5WS6) is not fully consistent with S_3 EXAFS data[9,46] (SI, Figures S1−S3), likely due to the unavoidable mixture of S states present in the XFEL microcrystals, with only a small fraction in the S_3 state. In fact, the apparently short O5−O6 distance suggested for the S_3 state can be accounted for in terms of partial occupation of O5 and O6 as determined by the composition of the mixture of S_1 and S_3 states. Here, we provide a structural interpretation of the reported difference Fourier features[13] based on QM/MM models.[6−9]

The OEC has four Mn ions and a Ca forming the oxomanganese cluster Mn_4CaO_5. The QM/MM S_3 model has an additional core O atom, arising from water binding during the S_2 to S_3 transition.[9] On the basis of data from the ammonia-

DOI: 10.1021/acsenergylett.7b00750
ACS Energy Lett. 2017, 2, 2299−2306

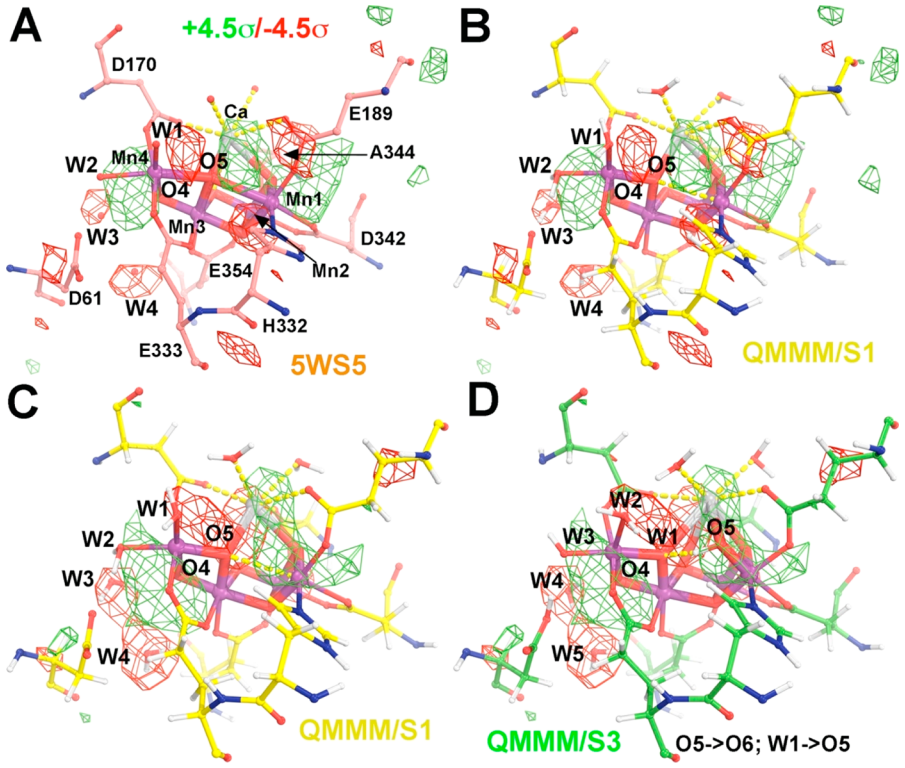

Figure 2. Observed difference Fourier maps between the $F_{obs}(5WS6/S_3) - F_{obs}(5WS5/S_1)$ XFEL data sets superimposed on the experimental S_1 model (A) and on the theoretical QM/MM S_1 model (B). (C,D) QM/MM-simulated difference Fourier maps between the $F_{simulated}(S_3) - F_{obs}(5WS5/S_1)$ pair, contoured at +4.5σ (green) and −4.5σ (red), superimposed onto the 5WS5 model (A, salmon), QM/MM S_1 model (B,C, yellow), and QM/MM S_3 model (D, green). When compared to the S_1 state, the S_3 model involves the following displacements: O5 → O6, W1 → O5, W2 → W1, W3 → W2, and W4 → W3. See Figures S5−S7 for additional stereodiagram views with numbering according to the PDB file reported for 5WS5.

bound S_2 QM/MM model,[12] formation of the S_3 state was proposed to occur through a carousel rearrangement (Scheme 1) involving water molecules W1, W2, and W3,[10] which correspond to water molecules #578, #523, and #527 in monomer A, respectively[13] (the original numbering reported in 5WS5 is provided in the SI, with uppercase one-letter labeling of amino acid residues for monomer A and with lowercase for monomer B). As shown in Scheme 1, oxidation of the OEC triggers binding of a water molecule (W3) to Mn4 from the so-called "narrow" channel (W3 is #527 in monomer A or Wx in our original nomenclature;[10] see the SI). W3 binding displaces W2 into the W1 position, and W1 is displaced into the O5 position. The O5 ligand is displaced toward a new position, becoming O6, using the nomenclature from Shen and co-workers.[13] The role of the narrow channel as a water delivery channel during the S_2−S_3 transition has also been supported by Capone et al.[16] and by Retegan et al.[23] The rearrangement associated with the carousel mechanism slightly displaces Ca toward O6 while Mn4 is slightly displaced away from Mn1, making room for the new O5 ligand. During the rearrangement, four out of six bidentate carboxylate ligands remain largely stationary (Figures 2 and S4−S7). However, E189 bound to Ca and Mn1 and D170 bound to Ca and Mn4 undergo torsion angle displacements to accommodate the new water molecule as O5 (Figures 2 and S4).

Figure 2C,D shows that the simulated S_3-*minus*-S_1 electron density difference based on QM/MM models[7,9] exhibits a positive feature (in green), extending from Ca to the new position of O5 as a ligand of Mn1 (O6 according to numbering by Shen), and a small displacement of Ca toward that new ligand. In addition, there are positive and negative features (in green and red, respectively) flanking the Mn4 center. No significant density difference features are observed at the W1 and W2 positions because there is no net change of electronic density produced by water ligand exchange. Furthermore, there is no significant negative peak behind Ca because there is concerted movement of a water molecule filling the depleted density upon Ca displacement.

The features revealed by the simulated electron density differences of QM/MM models are consistent with features in the observed isomorphous difference Fourier maps of XFEL data for $F_{obs}(5WS6/S_3)$ and $F_{obs}(5WS5/S_1)$, originally reported by Shen and colleagues and faithfully reproduced here (Figures 2A,B, S5, and S6).[13] Analogous to the QM/MM models, the XFEL difference Fourier map shows a small negative peak on W3 (#527) and a large negative peak next to W4 (#630).[13] These features suggest that W4 moves into the W3 position when W3 becomes a ligand of Mn4. However, other water molecules in the narrow channel do not refill the W4 position immediately. Remarkably, these features are observed for both monomers A and B.[13]

By using the same method, we have assessed the correctness of the QM/MM models as just described; we have also assessed whether the atomistic models of the S_1 and S_3 states proposed by Shen and co-workers were consistent with the outstanding features in the observed difference Fourier map that Shen and colleagues obtained and that we faithfully produced here, that is, whether their $F_{calc}(5WS6/S_3) - F_{calc}(5WS5/S_1)$ difference Fourier maps have reproduced the $F_{obs}(5WS6/S_3) - F_{obs}(5WS5/S_1)$ maps. The observed features in the S_3-*minus*-

DOI: 10.1021/acsenergylett.7b00750
ACS Energy Lett. 2017, 2, 2299−2306

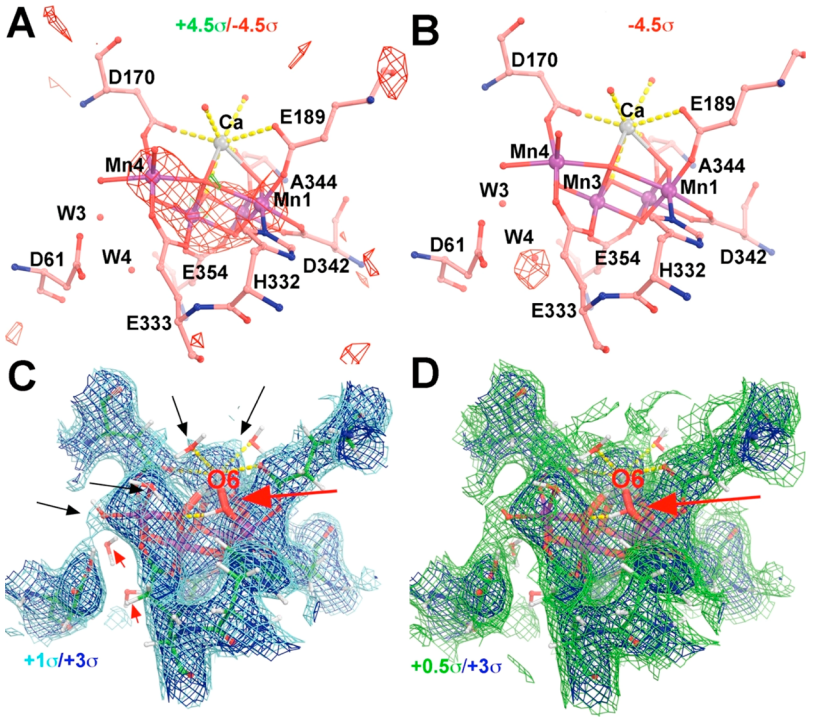

Figure 3. Assessment of the 5WS6 S_3 model using difference Fourier methods: (A) F_{calc}(5WS6/S_3) − F_{calc}(5WS5/S_1) or (B) F_{calc}(5WS6/S_3) − F_{obs}(5WS5/S_1) maps contoured at +4.5σ (green) and −4.5σ (red) and σ_A-weighted 2F_{obs} − F_{calc} map contoured at +1.0σ (cyan)/+3.0σ (blue) (C) and at +0.5σ (green)/+3.0σ (blue) (D). At the +1.0σ level (C), water ligands to the Ca and Mn centers (marked by black arrows) begin to emerge, but not O6 (red arrow) or W3 and W4 (small red arrows). There is no electron density visible for O6 at any contour level.

S_1 maps as discussed above are very robust because they are contributed by the observed amplitude differences from all of the reflections so that they are not much dependent on data of the selected resolution range used nor on any given set of model-calculated phases. That is, the observed difference Fourier features remain largely the same whether the model phases are from either F_{calc}(5WS6/S_3) or F_{calc}(5WS5/S_1). This is the reason why the observed difference Fourier maps are a very sensitive method to reveal subtle structural changes and have been extensively used by the crystallographic community for many decades.[41−43] However, we failed to obtain any robust features in the calculated difference Fourier maps that would be consistent with the observed features. Figure 3A shows that the calculated difference Fourier map using F_{calc}(5WS5/S_1) model phases, which represents one of many calculated difference Fourier maps that we have carefully examined, do not reproduce the observed map, suggesting that at least one of the two atomistic models (i.e., the S_3 model) does not correspond to the observed data. We have also examined the calculated difference Fourier maps using F_{calc}(5WS6/S_3) model phases with a different resolution range of data, for example, by excluding some very low resolution data. An exclusion of very low resolution data is relevant here because different model refinement programs may have slightly different bulk solvent correction algorithms that can result in different calculated structure factors at very low resolution, given the fact that the calculated structure factors were not deposited in the PDB and had to be regenerated here (see the Computational Methods section).

Because the 5WS5/S_1 model is consistent with the S_1 QM/MM model,[7,13] it is likely that the quality of the XFEL-derived 5WS6/S_3 model is questionable. This can be confirmed by using the difference Fourier map $F_{calc}(S_3) - F_{obs}(S_1)$ between the calculated structure factors (F_{calc}) of the 5WS6/S_3 model and the observed 5WS5/S_1 (F_{obs}) data (Figure 3B). The $F_{calc}(S_3) - F_{obs}(S_1)$ difference shown in Figure 3B shows a single negative peak at the W4 position, consistent with displacement of that water molecule during the S_1/S_3 transition.[13] However, none of the other observed features shown in Figure 2 are accounted for in Figure 3. Reciprocally, the hybrid F_{obs}(5WS6/S_3) − F_{calc}(5WS5/S_1) map was also calculated, and it is found that the features in this map largely reproduced the features in the observed difference Fourier maps (data not shown). This is another way to validate that the S_1 atomic model obtained by Shen and colleagues is indeed of reasonably good quality.

We further note that the σ_A-weighted 2F_{obs} − F_{calc} map based on the 5WS6/S_3 model does not show any electron density attributable to O6 at any contour level (Figure 3C,D). For example, several water ligands to Ca and some Mn centers are clearly visible in this map at the 1.0σ contour level, whereas O6 is not visible at 0.5σ (Figure 3C,D) or even at 0.01σ (data not shown). This observation suggests that the fraction of PSII cores converted to the S_3 state and recorded in the XFEL data is very low. Moreover, it is plausible that some of the observed density at the O5 position (Figure 2) in the F_{obs}(5WS6/S_3) − F_{obs}(5WS5/S_1) map may not come from the S_3 state but rather from other lower states. We thus conclude that the S_3 model might not actually have O5 and O6 at 1.5 Å from each other.[13] In any case, there is no conclusive evidence for an O−O bond formed in the S_3 state. The reason why one can see small subtle structural changes in the $F_{obs}(S_3) - F_{obs}(S_1)$ difference Fourier map but not in the $F_{obs}(S_3) - F_{calc}(S_3)$ difference Fourier maps [or in the $2F_{obs}(S_3) - F_{calc}(S_3)$ maps] is that the observed amplitude difference between the two states is only 6.8%, whereas the unbiased amplitude difference between the

DOI: 10.1021/acsenergylett.7b00750
ACS Energy Lett. 2017, 2, 2299−2306

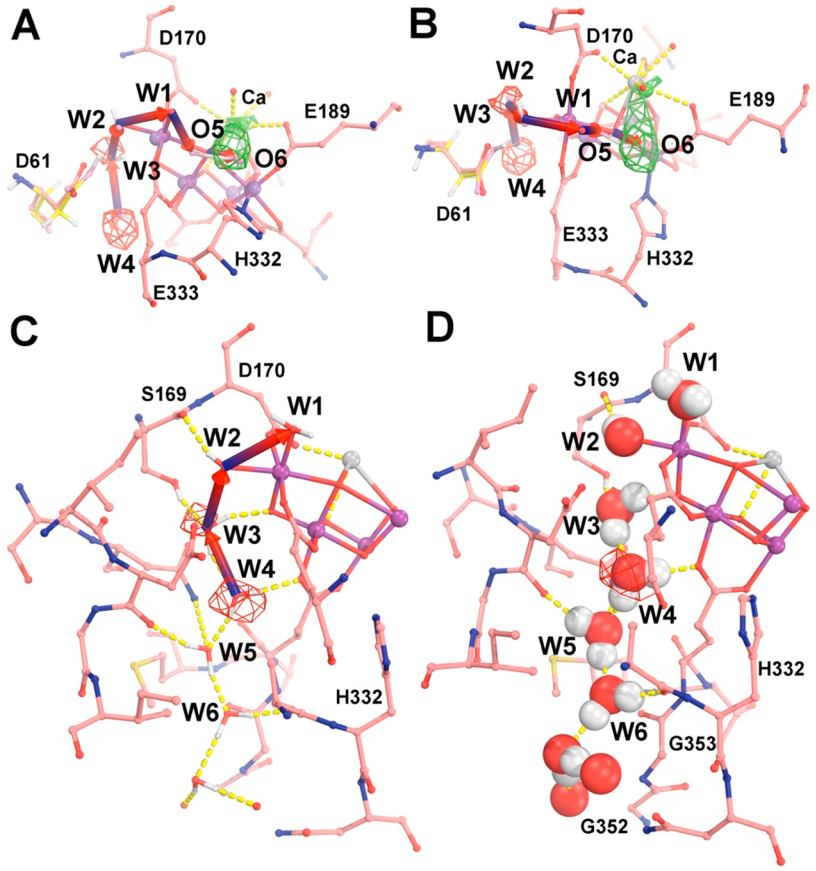

Figure 4. Single-file narrow water channel. (A,B) Two approximately orthogonal views of the 5WS5/S1 model (salmon, red, and blue) superimposed onto the edited F_{obs}(5WS6/S_3) − F_{obs}(5WS5/S_1) map contoured at +4.5σ (green) and −4.5σ (red) as well as with our QM/MM S_3 model (yellow, red, and blue), which contains the new O6 ligand. (C,D) Two representations of hydrogen-bonding interactions of water molecules in the single-file water channel. See Figure S8 for additional stereodiagram views.

calculated and observed amplitudes within the S_3 state (i.e., free *R* factor value) is 17.6% (see below for further discussion).[13]

W4 likely moves to the W3 site due to the immediate proximity when W3 takes the position of W2 (Figure 4A,B). As shown by the S_3 QM/MM model, the relative occupancy of each site is mostly determined by hydrogen-bonding interactions (Figures 4 and S8). W3 makes hydrogen bonds to Oγ of S169 and O4, while W2 makes bonds with D61 (Figure 4C,D). W4 makes a hydrogen bond with W5 and E354. All of these interactions are consistent with a preference of W4 to occupy the W3 site in the S_3 state. W5 might not immediately move into the vacant position of W4 because W4 has three hydrogen bonds, including the carbonyl O of D61, the side chain of N87, and a water molecule (Figure S8). Thus, we conjecture that an additional conformational change is necessary for W5 to take the position of W4. The energetics of potential movement of water molecules along this channel has been discussed,[19,20] although it has also been disfavored due to the limited water mobility.[47]

The density feature associated with W3, next to O4, disappears during the S_1 to S_3 transition (Figure 2A,B). Therefore, it seems unlikely that another water molecule would move next to O4 and become a substrate. Given the geometry constraints at that site, even molecular oxygen might not fit at the O4 position. Moreover, formation of an O−O bond at this position would be thermodynamically demanding because it requires breaking two coordination interactions of the μ-O4 bridge with rather unfavorable structural changes. Thus, we disfavor O4 as the site for O−O bond formation as suggested as a secondary possibility of the two possible models put forward by Shen and co-workers (two dashed circles in their Figure 4).[13] Instead, we favor the second water molecule to be located at the front end of the carousel cascade near the O5 and O6 positions, which corresponds to the first choice of Shen and colleagues but in different details,[13] interacting with Ca as suggested by oxygen isotope exchange measurements.[48]

In the S_0, S_1, and S_2 states, one water molecule is rapidly exchangeable, exhibiting the fastest rates within detectable experimental range, while another one is rather slow.[48] The fast water molecule is likely to be very weakly associated with the OEC, such as W1 on Mn4, while the slow one might be part of the OEC, tentatively assigned as the O5 species. In the S_0 state, O5 is a hydroxo, which should have a relatively higher exchangeable rate than those in the S_1 and S_2 states where O5 is an oxo species. However, considering that EPR signals show the presence of two S_2 state structures consistent with different O5 positions (i.e., as a ligand of either Mn1 or Mn4), it is reasonable to expect a higher exchangeable rate for O5 in S_2 when compared to the S_1 state.[48] In the S_3 state, W1 moves to the O5 position, consistent with the fast exchangeable water becoming very slow. At the same time, the original O5 species becomes O6, expected to have a slightly increased exchangeable rate.[48] These findings are particularly relevant to analysis of the reaction mechanism as directly compared to experimental data.

A lesson that we want to emphasize from this study is that, whereas technologies in X-ray crystallography have indeed been

DOI: 10.1021/acsenergylett.7b00750
ACS Energy Lett. 2017, 2, 2299−2306

advanced in the last few decades, the crystallographic foundation on how to assess whether the measured data contain useful structural information (i.e., above the noise level) remains unchanged, and the isomorphous difference Fourier method remains as a sensitive method to reveal subtle structural changes recorded in the measured differences in the diffraction data.[41−43] By all means, Shen and colleagues have done a superb job at data processing[13] and have provided high-quality XFEL data sets for PSII intermediates with cumulative Pearson split correlation coefficients ($CC_{1/2}$) of 99.4−99.7% and split intensity R factors of 5.4−6.2% for each data set that is comparable to the quality of conventional synchrotron data.[34,49,50] This permits Shen and colleagues to obtain useful structural information on the S_1 to S_3 state transition, which is reflected in the observed intensity difference of only 5.6% between the two data sets. Although the expected structural transition signals are indeed very weak, they are consistently present in each of 35 393 reflections at 2.35 Å resolution, making them collectively powerful and useful. For comparison, in another XFEL study on ammonia binding to PSII, the authors reported cumulative $CC_{1/2}$ values of 53.2% for the S_1 data set at 3.0 Å resolution and 54.2% for the two-flash NH_3 bound state at 2.8 Å resolution (the authors did not report intensity split R factors).[39] It is clear that these authors would have to put extra effort into their data processing procedures to improve the internal consistency indexes within each data set before they could conclude with certainty whether the diffraction data recorded any reliable structural information on ammonia binding to the OEC.

Chen and colleagues have done a superb job at XFEL data processing;[13] nevertheless, we do not find complete support of their interpretation, which was likely biased toward the "200 + 1 atom" open S_3 model generated by Li and Siegbahn (Figure S9A),[51] with a hallmark intermediate O5−H−O6 configuration where O6 is a newly added water substrate (+1). In their energy-minimized model, Li and Siegbahn relaxed all of the truncated protein side chains (and therefore all water molecules nearby) that freely reposition. The relaxation resulted in displacement of the H332 side chain by about 2.30 Å, relative to the experimental coordinates of the 5WS5 mode from our S_3 model, as well as a large displacement of the Cl^- ion by 0.73 Å (Figure S9) and water molecules. Unfortunately, these displacements are not consistent with the experimental features observed in the difference Fourier maps obtained by Chen and colleagues.[13] While large movements of protein side chains during the S_1 to S_3 state transition have been suggested based on low-resolution XFEL data,[35] that interpretation did not take into account possible effects of Fourier series termination.[9] Furthermore, large displacements are not consistent with the much higher resolution, better-quality, new XFEL data obtained by Shen and co-workers.[13] Moreover, even though the Li and Siegbahn model may have accounted for the selected Mn−Mn distances derived from the EXAFS data, their model has not been shown to reproduce the EXAFS spectra just like many other alternative models (Figures S1−S3).[12] Therefore, our model and the carousel mechanism seem to remain most consistent with XFEL data and the EXAFS spectra, as compared to other suggested models.

COMPUTATIONAL METHODS

Crystallographic analysis was carried out using the program CCP4 suite and displayed using the graphics Coot.[52,53] When the OEC and its protein ligands from the QM/MM model were reinserted into an experimental atomic model, the uniform atomic B factor was kept the same for the mean B factor for the replaced part of the model. The QM level of our original S_3 QM/MM model did not include W3 and W4. Therefore, reoptimization of the S_3 QM/MM with W4 displaced to the W3 position led to a model that is even in better agreement with the published EXAFS data for the S_3 state (Figures S2 and S3). The calculated structure factors were obtained from atomic models using Refmac5 by setting the zero cycle rigid-body refinement option.[54] The correctness of the structure factor calculation has been verified by visual inspection of both $2F_{obs} - F_{calc}$ and $F_{obs} - F_{calc}$ maps and by comparison with the reported statistical values such as amplitude differences.

For comparisons with experiments, we note that the features of the difference Fourier maps do not provide how much S_3 was formed by the two flashes. Difference features of the same kind would be observed regardless of whether the transition is 100% complete or, for example, only 20% because the unchanged portion between the two structures cancels out in both cases. The only difference between 100 or 20% completion would be that the peak heights in the latter would be reduced 5-fold relative to the former. In the PDB 5WS6/S_3 atomic coordinate file, Shen and colleagues modeled two alternative conformations of 20:80% for a mixed $CaMn_4O_5$ cluster in each monomer.[13] Yet, the occupancy of O6 was modeled as 40%, which did not correspond to either state of the cluster. The basis of this discrepancy was not discussed in their publication and remains unknown. If O6 is part of part of a minor species, it has an extra O6 relative to the species by 20%. If O6 is part of the major species (which the coordinates imply), 40% of the species lacks O6, which leads to another question: can the S_3 state exist without O6 binding? Another aspect that should be noted is that XFEL crystallography is a :diffraction-while-destruction" technique.[34] Therefore, the atomic scattering factors do not necessarily correspond to those of conventional synchrotron radiation. Nevertheless, the isomorphous $F_{obs} - F_{obs}$ difference Fourier maps should partially cancel some of the systematic errors due to a change in atomic scattering factors.

ASSOCIATED CONTENT

Supporting Information

The Supporting Information is available free of charge on the ACS Publications website at DOI: 10.1021/acsenergylett.7b00750.

Description of QM/MM models, description of EXAFS analysis, electron density map analysis, additional references, and updated S_3 state coordinates (PDF)

AUTHOR INFORMATION

Corresponding Author

*E-mail: victor.batista@yale.edu.

ORCID

Gary W. Brudvig: 0000-0002-7040-1892

Victor S. Batista: 0000-0002-3262-1237

Notes

The authors declare no competing financial interest.

ACKNOWLEDGMENTS

The authors acknowledge support by the U.S. Department of Energy, Office of Science, Office of Basic Energy Sciences,

DOI: 10.1021/acsenergylett.7b00750
ACS Energy Lett. 2017, 2, 2299−2306

Division of Chemical Sciences, Geosciences, and Biosciences, Photosynthetic Systems. Experimental work was funded by Grant DE-FG02-05ER15646 (G.W.B.), computational work was funded by Grant DESC0001423 (V.S.B), and crystallographic study was supported by National Institutes of Health Grant P01 GM022778 (J.W).

REFERENCES

(1) McEvoy, J. P.; Brudvig, G. W. Water-splitting chemistry of photosystem II. *Chem. Rev.* **2006**, *106* (11), 4455−4483.
(2) Cox, N.; Pantazis, D. A.; Neese, F.; Lubitz, W. Biological Water Oxidation. *Acc. Chem. Res.* **2013**, *46* (7), 1588−1596.
(3) Shen, J. R. The Structure of Photosystem II and the Mechanism of Water Oxidation in Photosynthesis. *Annu. Rev. Plant Biol.* **2015**, *66* (66), 23−48.
(4) Joliot, P.; Kok, B., Oxygen evolution in photosynthesis. In *Bioenergetics of Photosynthesis*; Govindjee, Ed. Academic Press: New York, 1975; pp 387−412.
(5) Kok, B.; Forbush, B.; Mcgloin, M. Cooperation of Charges in Photosynthetic O2 Evolution-I. A Linear Four Step Mechanism. *Photochem. Photobiol.* **1970**, *11* (6), 457−475.
(6) Pal, R.; Negre, C. F. A.; Vogt, L.; Pokhrel, R.; Ertem, M. Z.; Brudvig, G. W.; Batista, V. S. S-0-State Model of the Oxygen-Evolving Complex of Photosystem II. *Biochemistry* **2013**, *52* (44), 7703−7706.
(7) Luber, S.; Rivalta, I.; Umena, Y.; Kawakami, K.; Shen, J. R.; Kamiya, N.; Brudvig, G. W.; Batista, V. S. S-1-State Model of the O-2-Evolving Complex of Photosystem II. *Biochemistry* **2011**, *50* (29), 6308−6311.
(8) Askerka, M.; Wang, J.; Brudvig, G. W.; Batista, V. S. Structural Changes in the Oxygen-Evolving Complex of Photosystem II Induced by the S1 to S2 Transition: A Combined XRD and QM/MM Study. *Biochemistry* **2014**, *53* (44), 6860−6862.
(9) Askerka, M.; Wang, J.; Vinyard, D. J.; Brudvig, G. W.; Batista, V. S. S3 State of the O2-Evolving Complex of Photosystem II: Insights from QM/MM, EXAFS, and Femtosecond X-ray Diffraction. *Biochemistry* **2016**, *55* (7), 981−4.
(10) Askerka, M.; Brudvig, G. W.; Batista, V. S. The O2-Evolving Complex of Photosystem II: Recent Insights from Quantum Mechanics/Molecular Mechanics (QM/MM), Extended X-ray Absorption Fine Structure (EXAFS), and Femtosecond X-ray Crystallography Data. *Acc. Chem. Res.* **2017**, *50* (1), 41−48.
(11) Shoji, M.; Isobe, H.; Nakajima, T.; Shigeta, Y.; Suga, M.; Akita, F.; Shen, J. R.; Yamaguchi, K. Large-scale QM/MM calculations of the CaMn4O5 cluster in the S3 state of the oxygen evolving complex of photosystem II. Comparison between water-inserted and no water-inserted structures. *Faraday Discuss.* **2017**, *198*, 83−106.
(12) Askerka, M.; Vinyard, D. J.; Brudvig, G. W.; Batista, V. S. NH3 Binding to the S2 State of the O2-Evolving Complex of Photosystem II: Analogue to H2O Binding during the S2 –> S3 Transition. *Biochemistry* **2015**, *54* (38), 5783−6.
(13) Suga, M.; Akita, F.; Sugahara, M.; Kubo, M.; Nakajima, Y.; Nakane, T.; Yamashita, K.; Umena, Y.; Nakabayashi, M.; Yamane, T.; Nakano, T.; Suzuki, M.; Masuda, T.; Inoue, S.; Kimura, T.; Nomura, T.; Yonekura, S.; Yu, L. J.; Sakamoto, T.; Motomura, T.; Chen, J. H.; Kato, Y.; Noguchi, T.; Tono, K.; Joti, Y.; Kameshima, T.; Hatsui, T.; Nango, E.; Tanaka, R.; Naitow, H.; Matsuura, Y.; Yamashita, A.; Yamamoto, M.; Nureki, O.; Yabashi, M.; Ishikawa, T.; Iwata, S.; Shen, J. R. Light-induced structural changes and the site of O=O bond formation in PSII caught by XFEL. *Nature* **2017**, *543* (7643), 131−135.
(14) Cox, N.; Messinger, J. Reflections on substrate water and dioxygen formation. *Biochim. Biophys. Acta, Bioenerg.* **2013**, *1827* (8−9), 1020−30.
(15) Retegan, M.; Pantazis, D. A. Interaction of methanol with the oxygen-evolving complex: atomistic models, channel identification, species dependence, and mechanistic implications. *Chem. Sci.* **2016**, *7* (10), 6463−6476.
(16) Capone, M.; Narzi, D.; Bovi, D.; Guidoni, L. Mechanism of Water Delivery to the Active Site of Photosystem II along the S(2) to S(3) Transition. *J. Phys. Chem. Lett.* **2016**, *7* (3), 592−6.
(17) Perez Navarro, M.; Ames, W. M.; Nilsson, H.; Lohmiller, T.; Pantazis, D. A.; Rapatskiy, L.; Nowaczyk, M. M.; Neese, F.; Boussac, A.; Messinger, J.; Lubitz, W.; Cox, N. Ammonia binding to the oxygen-evolving complex of photosystem II identifies the solvent-exchangeable oxygen bridge (mu-oxo) of the manganese tetramer. *Proc. Natl. Acad. Sci. U. S. A.* **2013**, *110* (39), 15561−6.
(18) Lohmiller, T.; Krewald, V.; Navarro, M. P.; Retegan, M.; Rapatskiy, L.; Nowaczyk, M. M.; Boussac, A.; Neese, F.; Lubitz, W.; Pantazis, D. A.; Cox, N. Structure, ligands and substrate coordination of the oxygen-evolving complex of photosystem II in the S2 state: a combined EPR and DFT study. *Phys. Chem. Chem. Phys.* **2014**, *16* (24), 11877−92.
(19) Vassiliev, S.; Zaraiskaya, T.; Bruce, D. Molecular dynamics simulations reveal highly permeable oxygen exit channels shared with water uptake channels in photosystem II. *Biochim. Biophys. Acta, Bioenerg.* **2013**, *1827* (10), 1148−55.
(20) Vassiliev, S.; Zaraiskaya, T.; Bruce, D. Exploring the energetics of water permeation in photosystem II by multiple steered molecular dynamics simulations. *Biochim. Biophys. Acta, Bioenerg.* **2012**, *1817* (9), 1671−8.
(21) Guo, Y.; He, L. L.; Zhao, D. X.; Gong, L. D.; Liu, C.; Yang, Z. Z. How does ammonia bind to the oxygen-evolving complex in the S2 state of photosynthetic water oxidation? Theoretical support and implications for the W1 substitution mechanism. *Phys. Chem. Chem. Phys.* **2016**, *18* (46), 31551−31565.
(22) Guo, Y.; Li, H.; He, L. L.; Zhao, D. X.; Gong, L. D.; Yang, Z. Z. The open-cubane oxo-oxyl coupling mechanism dominates photosynthetic oxygen evolution: a comprehensive DFT investigation on O-O bond formation in the S4 state. *Phys. Chem. Chem. Phys.* **2017**, *19* (21), 13909−13923.
(23) Retegan, M.; Krewald, V.; Mamedov, F.; Neese, F.; Lubitz, W.; Cox, N.; Pantazis, D. A. A five-coordinate Mn (iv) intermediate in biological water oxidation: spectroscopic signature and a pivot mechanism for water binding. *Chem. Sci.* **2016**, *7*, 72−84.
(24) Umena, Y.; Kawakami, K.; Shen, J.-R.; Kamiya, N. Crystal structure of oxygen-evolving Photosystem II at a resolution of 1.9 angstrom. *Nature* **2011**, *473* (7345), 55−60.
(25) Tanaka, A.; Fukushima, Y.; Kamiya, N. Two Different Structures of the Oxygen-Evolving Complex in the Same Polypeptide Frameworks of Photosystem II. *J. Am. Chem. Soc.* **2017**, *139* (5), 1718−1721.
(26) Vogt, L.; Ertem, M. Z.; Pal, R.; Brudvig, G. W.; Batista, V. S. Computational insights on crystal structures of the oxygen-evolving complex of photosystem II with either Ca(2+) or Ca(2+) substituted by Sr(2+). *Biochemistry* **2015**, *54* (3), 820−5.
(27) Yano, J.; Kern, J.; Irrgang, K. D.; Latimer, M. J.; Bergmann, U.; Glatzel, P.; Pushkar, Y.; Biesiadka, J.; Loll, B.; Sauer, K.; Messinger, J.; Zouni, A.; Yachandra, V. K. X-ray damage to the Mn4Ca complex in single crystals of photosystem II: a case study for metalloprotein crystallography. *Proc. Natl. Acad. Sci. U. S. A.* **2005**, *102* (34), 12047−52.
(28) Wang, J. X-ray radiation-induced addition of oxygen atoms to protein residues. *Protein Sci.* **2016**, *25* (8), 1407−19.
(29) Meents, A.; Dittrich, B.; Gutmann, S. A new aspect of specific radiation damage: hydrogen abstraction from organic molecules. *J. Synchrotron Radiat.* **2009**, *16* (2), 183−90.
(30) Meents, A.; Gutmann, S.; Wagner, A.; Schulze-Briese, C. Origin and temperature dependence of radiation damage in biological samples at cryogenic temperatures. *Proc. Natl. Acad. Sci. U. S. A.* **2010**, *107* (3), 1094−9.
(31) Suga, M.; Akita, F.; Hirata, K.; Ueno, G.; Murakami, H.; Nakajima, Y.; Shimizu, T.; Yamashita, K.; Yamamoto, M.; Ago, H.; Shen, J. R. Native structure of photosystem II at 1.95 A resolution viewed by femtosecond X-ray pulses. *Nature* **2014**, *517* (7532), 99−103.
(32) Young, I. D.; Ibrahim, M.; Chatterjee, R.; Gul, S.; Fuller, F. D.; Koroidov, S.; Brewster, A. S.; Tran, R.; Alonso-Mori, R.; Kroll, T.;

DOI: 10.1021/acsenergylett.7b00750
ACS Energy Lett. 2017, 2, 2299−2306

Michels-Clark, T.; Laksmono, H.; Sierra, R. G.; Stan, C. A.; Hussein, R.; Zhang, M.; Douthit, L.; Kubin, M.; de Lichtenberg, C.; Vo Pham, L.; Nilsson, H.; Cheah, M. H.; Shevela, D.; Saracini, C.; Bean, M. A.; Seuffert, I.; Sokaras, D.; Weng, T. C.; Pastor, E.; Weninger, C.; Fransson, T.; Lassalle, L.; Brauer, P.; Aller, P.; Docker, P. T.; Andi, B.; Orville, A. M.; Glownia, J. M.; Nelson, S.; Sikorski, M.; Zhu, D.; Hunter, M. S.; Lane, T. J.; Aquila, A.; Koglin, J. E.; Robinson, J.; Liang, M.; Boutet, S.; Lyubimov, A. Y.; Uervirojnangkoorn, M.; Moriarty, N. W.; Liebschner, D.; Afonine, P. V.; Waterman, D. G.; Evans, G.; Wernet, P.; Dobbek, H.; Weis, W. I.; Brunger, A. T.; Zwart, P. H.; Adams, P. D.; Zouni, A.; Messinger, J.; Bergmann, U.; Sauter, N. K.; Kern, J.; Yachandra, V. K.; Yano, J. Structure of photosystem II and substrate binding at room temperature. *Nature* **2016**, *540* (7633), 453−457.

(33) Amin, M.; Badawi, A.; Obayya, S. S. Radiation Damage in XFEL: Case study from the oxygen-evolving complex of Photosystem II. *Sci. Rep.* **2016**, *6*, 36492.

(34) Wang, J. Destruction-and-diffraction by X-ray free-electron laser. *Protein Sci.* **2016**, *25* (9), 1585−92.

(35) Kupitz, C.; Basu, S.; Grotjohann, I.; Fromme, R.; Zatsepin, N. A.; Rendek, K. N.; Hunter, M. S.; Shoeman, R. L.; White, T. A.; Wang, D.; James, D.; Yang, J. H.; Cobb, D. E.; Reeder, B.; Sierra, R. G.; Liu, H.; Barty, A.; Aquila, A. L.; Deponte, D.; Kirian, R. A.; Bari, S.; Bergkamp, J. J.; Beyerlein, K. R.; Bogan, M. J.; Caleman, C.; Chao, T. C.; Conrad, C. E.; Davis, K. M.; Fleckenstein, H.; Galli, L.; Hau-Riege, S. P.; Kassemeyer, S.; Laksmono, H.; Liang, M.; Lomb, L.; Marchesini, S.; Martin, A. V.; Messerschmidt, M.; Milathianaki, D.; Nass, K.; Ros, A.; Roy-Chowdhury, S.; Schmidt, K.; Seibert, M.; Steinbrener, J.; Stellato, F.; Yan, L.; Yoon, C.; Moore, T. A.; Moore, A. L.; Pushkar, Y.; Williams, G. J.; Boutet, S.; Doak, R. B.; Weierstall, U.; Frank, M.; Chapman, H. N.; Spence, J. C.; Fromme, P. Serial time-resolved crystallography of photosystem II using a femtosecond X-ray laser. *Nature* **2014**, *513* (7517), 261−5.

(36) Kern, J.; Alonso-Mori, R.; Tran, R.; Hattne, J.; Gildea, R. J.; Echols, N.; Glockner, C.; Hellmich, J.; Laksmono, H.; Sierra, R. G.; Lassalle-Kaiser, B.; Koroidov, S.; Lampe, A.; Han, G.; Gul, S.; Difiore, D.; Milathianaki, D.; Fry, A. R.; Miahnahri, A.; Schafer, D. W.; Messerschmidt, M.; Seibert, M. M.; Koglin, J. E.; Sokaras, D.; Weng, T. C.; Sellberg, J.; Latimer, M. J.; Grosse-Kunstleve, R. W.; Zwart, P. H.; White, W. E.; Glatzel, P.; Adams, P. D.; Bogan, M. J.; Williams, G. J.; Boutet, S.; Messinger, J.; Zouni, A.; Sauter, N. K.; Yachandra, V. K.; Bergmann, U.; Yano, J. Simultaneous femtosecond X-ray spectroscopy and diffraction of photosystem II at room temperature. *Science* **2013**, *340* (6131), 491−5.

(37) Kern, J.; Alonso-Mori, R.; Hellmich, J.; Tran, R.; Hattne, J.; Laksmono, H.; Glockner, C.; Echols, N.; Sierra, R. G.; Sellberg, J.; Lassalle-Kaiser, B.; Gildea, R. J.; Glatzel, P.; Grosse-Kunstleve, R. W.; Latimer, M. J.; McQueen, T. A.; DiFiore, D.; Fry, A. R.; Messerschmidt, M.; Miahnahri, A.; Schafer, D. W.; Seibert, M. M.; Sokaras, D.; Weng, T. C.; Zwart, P. H.; White, W. E.; Adams, P. D.; Bogan, M. J.; Boutet, S.; Williams, G. J.; Messinger, J.; Sauter, N. K.; Zouni, A.; Bergmann, U.; Yano, J.; Yachandra, V. K. Room temperature femtosecond X-ray diffraction of photosystem II microcrystals. *Proc. Natl. Acad. Sci. U. S. A.* **2012**, *109* (25), 9721−6.

(38) Kern, J.; Tran, R.; Alonso-Mori, R.; Koroidov, S.; Echols, N.; Hattne, J.; Ibrahim, M.; Gul, S.; Laksmono, H.; Sierra, R. G.; Gildea, R. J.; Han, G.; Hellmich, J.; Lassalle-Kaiser, B.; Chatterjee, R.; Brewster, A. S.; Stan, C. A.; Glockner, C.; Lampe, A.; DiFiore, D.; Milathianaki, D.; Fry, A. R.; Seibert, M. M.; Koglin, J. E.; Gallo, E.; Uhlig, J.; Sokaras, D.; Weng, T. C.; Zwart, P. H.; Skinner, D. E.; Bogan, M. J.; Messerschmidt, M.; Glatzel, P.; Williams, G. J.; Boutet, S.; Adams, P. D.; Zouni, A.; Messinger, J.; Sauter, N. K.; Bergmann, U.; Yano, J.; Yachandra, V. K. Taking snapshots of photosynthetic water oxidation using femtosecond X-ray diffraction and spectroscopy. *Nat. Commun.* **2014**, *5*, 4371.

(39) Young, I. D.; Ibrahim, M.; Chatterjee, R.; Gul, S.; Fuller, F. D.; Koroidov, S.; Brewster, A. S.; Tran, R.; Alonso-Mori, R.; Kroll, T.; Michels-Clark, T.; Laksmono, H.; Sierra, R. G.; Stan, C. A.; Hussein, R.; Zhang, M.; Douthit, L.; Kubin, M.; de Lichtenberg, C.; Vo Pham, L.; Nilsson, H.; Cheah, M. H.; Shevela, D.; Saracini, C.; Bean, M. A.; Seuffert, I.; Sokaras, D.; Weng, T. C.; Pastor, E.; Weninger, C.; Fransson, T.; Lassalle, L.; Brauer, P.; Aller, P.; Docker, P. T.; Andi, B.; Orville, A. M.; Glownia, J. M.; Nelson, S.; Sikorski, M.; Zhu, D.; Hunter, M. S.; Lane, T. J.; Aquila, A.; Koglin, J. E.; Robinson, J.; Liang, M.; Boutet, S.; Lyubimov, A. Y.; Uervirojnangkoorn, M.; Moriarty, N. W.; Liebschner, D.; Afonine, P. V.; Waterman, D. G.; Evans, G.; Wernet, P.; Dobbek, H.; Weis, W. I.; Brunger, A. T.; Zwart, P. H.; Adams, P. D.; Zouni, A.; Messinger, J.; Bergmann, U.; Sauter, N. K.; Kern, J.; Yachandra, V. K.; Yano, J. Structure of photosystem II and substrate binding at room temperature. *Nature* **2016**, *540*, 453−457.

(40) Wang, J.; Askerka, M.; Brudvig, G. W.; Batista, V. S. Insights into Photosystem II from Isomorphous Difference Fourier Maps of Femtosecond X-ray Diffraction Data and Quantum Mechanics/Molecular Mechanics Structural Models. *ACS Energy Lett.* **2017**, *2* (2), 397−407.

(41) Rould, M. A.; Carter, C. W., Jr. Isomorphous difference methods. *Methods Enzymol.* **2003**, *374*, 145−63.

(42) Kraut, J. Structural Studies with X-Rays. *Annu. Rev. Biochem.* **1965**, *34*, 247−68.

(43) Stryer, L.; Kendrew, J. C.; Watson, H. C. The Mode of Attachment of the Azide Ion to Sperm Whale Metmyoglobin. *J. Mol. Biol.* **1964**, *8*, 96−104.

(44) Dau, H.; Grundmeier, A.; Loja, P.; Haumann, M. On the structure of the manganese complex of photosystem II: extended-range EXAFS data and specific atomic-resolution models for four S-states. *Philos. Trans. R. Soc., B* **2008**, *363* (1494), 1237−1243.

(45) Askerka, M.; Vinyard, D. J.; Wang, J. M.; Brudvig, G. W.; Batista, V. S. Analysis of the Radiation-Damage-Free X-ray Structure of Photosystem II in Light of EXAFS and QM/MM Data. *Biochemistry* **2015**, *54* (9), 1713−1716.

(46) Haumann, M.; Muller, C.; Liebisch, P.; Iuzzolino, L.; Dittmer, J.; Grabolle, M.; Neisius, T.; Meyer-Klaucke, W.; Dau, H. Structural and oxidation state changes of the Photosystem II manganese complex in four transitions of the water oxidation cycle (S0 -> S1, S1 -> S2, S2 -> S3, and S3,4 -> S0) characterized by X-ray absorption spectroscopy at 20 K and room temperature. *Biochemistry* **2005**, *44* (6), 1894−1908.

(47) Saito, K.; Rutherford, A. W.; Ishikita, H. Energetics of proton release on the first oxidation step in the water-oxidizing enzyme. *Nat. Commun.* **2015**, *6*, 8488.

(48) Hillier, W.; Wydrzynski, T. O-18-Water exchange in photosystem II: Substrate binding and intermediates of the water splitting cycle. *Coord. Chem. Rev.* **2008**, *252* (3−4), 306−317.

(49) Wang, J.; Wing, R. A. Diamonds in the rough: a strong case for the inclusion of weak-intensity X-ray diffraction data. *Acta Crystallogr., Sect. D: Biol. Crystallogr.* **2014**, *70*, 1491−7.

(50) Karplus, P. A.; Diederichs, K. Assessing and maximizing data quality in macromolecular crystallography. *Curr. Opin. Struct. Biol.* **2015**, *34*, 60−8.

(51) Li, X. C.; Siegbahn, P. E. M. Alternative mechanisms for O-2 release and O-O bond formation in the oxygen evolving complex of photosystem II. *Phys. Chem. Chem. Phys.* **2015**, *17* (18), 12168−12174.

(52) Winn, M. D.; Ballard, C. C.; Cowtan, K. D.; Dodson, E. J.; Emsley, P.; Evans, P. R.; Keegan, R. M.; Krissinel, E. B.; Leslie, A. G.; McCoy, A.; McNicholas, S. J.; Murshudov, G. N.; Pannu, N. S.; Potterton, E. A.; Powell, H. R.; Read, R. J.; Vagin, A.; Wilson, K. S. Overview of the CCP4 suite and current developments. *Acta Crystallogr., Sect. D: Biol. Crystallogr.* **2011**, *67*, 235−242.

(53) Emsley, P.; Cowtan, K. Coot: model-building tools for molecular graphics. *Acta Crystallogr., Sect. D: Biol. Crystallogr.* **2004**, *60*, 2126−2132.

(54) Murshudov, G. N.; Skubak, P.; Lebedev, A. A.; Pannu, N. S.; Steiner, R. A.; Nicholls, R. A.; Winn, M. D.; Long, F.; Vagin, A. A. REFMAC5 for the refinement of macromolecular crystal structures. *Acta Crystallogr., Sect. D: Biol. Crystallogr.* **2011**, *67*, 355−367.

DOI: 10.1021/acsenergylett.7b00750
ACS Energy Lett. 2017, 2, 2299−2306